TUTA/IOE/PCU

Journal of the Institute of Engineering
*January 2019, Vol. **15 (No. 1):** 25-36*

Numerical Investigation of a Steam Nozzle with Focus on Non-Equilibrium Condensation and Unsteady Flow Behavior

Hari Bahadur Dura
Department of Mechanical Engineering, Pulchowk Campus, IOE, Tribhuvan University, Nepal
Corresponding author: *duraharis@gmail.com*

Received: *Sep 20, 2018* **Revised:** *Dec 25, 2018* **Accepted:** *Jan 2, 2019*

Abstract: Present work analyses the condensation of superheated water vapor in supersonic Barschdorff nozzle. The influence of pneumatic mounts in 3D laval nozzle is analyzed using steady and unsteady two phase non-equilibrium condensation steam flow model in Ansys CFX16. Mesh independency studies in 2D model showed that at a lower inlet total temperature and very fine mesh (e.g. 100.2°C and 77k mesh elements) there is problem with the convergence using steady simulation. This is possibly due to the ability of very fine mesh to capture the small flow unsteadiness. The variation in location of Wilson's point, Wilson's pressure and maximum sub-cooling rate at the centerline of the nozzle is below 1.5%. The 2D CFD nucleation rate is 50% stronger and droplet diameter is 18% higher compared to the 3D CFD results. The deviation in nucleation rate and droplet diameter at nozzle outlet is the result of dissipation due to wing structure in the 3D model. Nucleation zone predicted by Ansys CFX16 is far upstream the experimental one. Different correction factors in modified nucleation model were used to fit the computed pressure distribution with the experimental one. The correction factor is dependent on boundary conditions and nozzle profile. It is thus concluded that the significance of such correction factor is not unique.

Keywords: Droplet growth, Nucleation rate, Steam condensation, Two-phase flow

1. Introduction

Historical Background: Low pressure turbines are susceptible to the condensation process that accounts for 25.5% of the total losses. Practically in all low pressure steam turbines that are used for electrical power generation the steam in the last turbine stages reaches saturated conditions. In order to maximize the cycle efficiency of the steam turbine about 10% to 12% wetness fraction at the outlet is necessary [14]. Impact velocity, droplet size, impacting droplet flow rate, and hardness of the target material are the most important parameters in rotor blade erosion caused by the impact of water droplets. It was also observed that the impact angle is not important in water droplet erosion. However, it influences the erosion before craters are formed on the target surface [17]. In operational turbines variation of nucleation zone exists along radial, circumferential and axial direction. Analysis requires to resolve the coupled transient

aerodynamics and condensation process. And it is impossible to measure the pressure and droplet size distribution along the rotor blade passage. Realizing the complexity of condensation process in real operational turbines, we simplify our study to stationary cascade. But even in these cascades nucleation zone varies in axial and circumferential direction. Flow in cascade is coupled system of aerodynamics and condensation process. It is still very difficult to measure the pressure and droplet size distribution along the streamlines in the cascades as the path is curved. Further simplification of the cascades leads to the nozzles where the aerodynamic influence is negligible. Variation of nucleation zone is along axial direction in nozzles. Also the measurement of the pressure and droplet size along the channel axis is technically and economically feasible [2, 3, 9, 12, 18, 22, 23].

Condensation Thermodynamics: Homogenous condensation assumes generation of mono-disperse particles as a result of spontaneous condensation. Once condensation sets in the analysis consists of the expansion process of both the super-cooled vapor phase and condensed liquid phase. Variables that define two phase flow are related by the conservation of mass, momentum and energy of the whole system. Also the nucleation and droplet growth model determines the important features of two phase flow. Consider a vapor expanded from a superheated state such that it crosses the saturation line. For relatively fast expansion process, the vapor will not have enough time to adjust itself immediately for the condensation. And hence it will remain as vapor and continues to expand like superheated vapor even after crossing the saturation line.

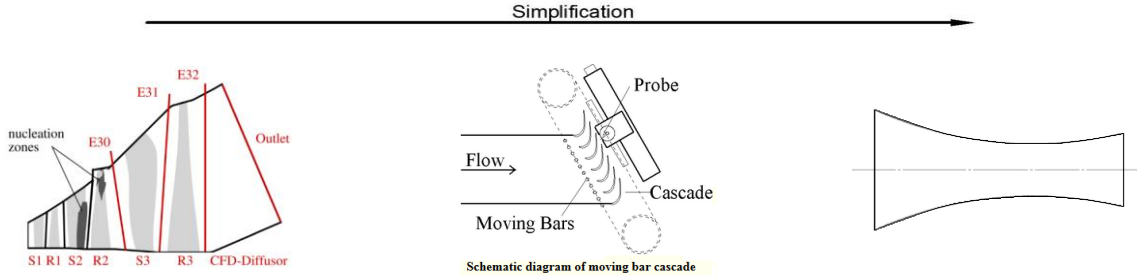

3D Turbine [Source: 16] | Cascade – Source: Whittle Laboratory | Laval nozzle

Fig. 1: Simplification of experimental investigation of condensation process

This phase of vapor in a meta-stable equilibrium condition behaves like superheated vapor and referred to as 'super-cooled vapor' or 'Super-cooled vapor'. It is also called as 'supersaturated' or 'sub-cooled'. At certain point called Wilson point (location where $p' \,\&\, p'' > 0$, Fig. 2) where the super-cooled vapor can no longer hold its meta-stable equilibrium condition, further expansion causes a sudden collapse of the super-saturated with the formation of nearly mono-disperse droplets appearing in the form of a fog. This process is called homogeneous condensation which takes place in the absence of any foreign nuclei. The release of latent heat during condensation results in an adiabatic flow with an increase in pressure [16, 21, 24].

Fig. 2 shows the phenomenon of supersaturated steam condensation in a Laval nozzle. The h-s diagram on the top shows the isentropic expansion vapor from initial stagnation conditions to crossing the saturation line and staying in a supersaturated state until at pressure when suddenly

spontaneous condensation occurs. The release of latent heat causes an increase in temperature, pressure and entropy. Often this sudden rise in pressure is often misinterpreted as condensation shock. The steepness of the pressure rise is because of the condensation process. The strength of the steepness depends on the strength of condensation or nucleation rate, which again is influenced by the geometry of the nozzle and stagnation conditions or boundary conditions. For a low expansion rate nozzle the pressure rise is not abrupt. The super-cooling decreases as the vapor temperature, pressure and entropy increase. Consequently, the super-cooled vapor becomes closer and closer to its equilibrium state. The spontaneous condensation process takes place instantaneously. Eventually at the end of spontaneous condensation the pressure is attained. After that the super-cooled vapor will almost achieve equilibrium state. Further expansion downstream would be an equilibrium isentropic expansion [8, 15]. For given inlet total pressure, with an increase in total inlet temperature the condensation zone moves upstream the nozzle, also the strength of the condensation increases. As the total inlet temperature decreases the flow tends to become more and more unstable. This unstable force can be significantly important in the health monitoring of the turbine blades.

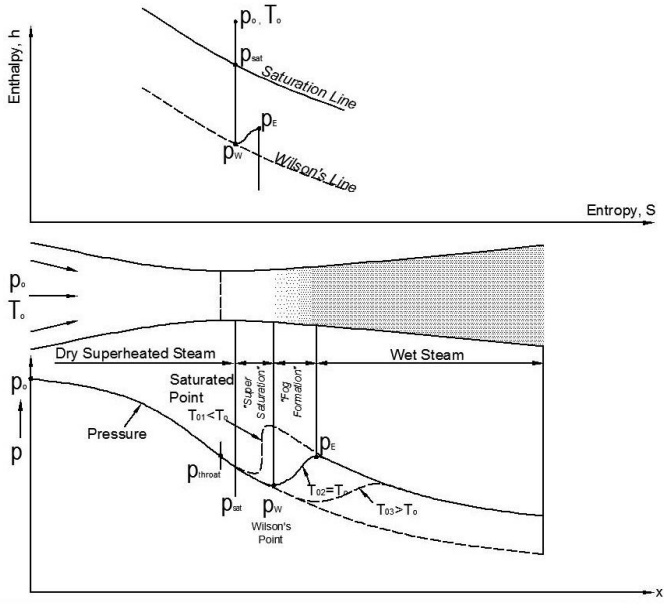

Fig. 2: Condensation in nozzle

2. Two-Phase Flow Modeling

2.1 Governing Equations

The real gas properties in the steam are calculated from IAPWS standard, while the meta-stable region is treated by extrapolations from the superheated region [20]. The usual constraint for the volume fractions of the phases is

$$\phi_V + \sum_{d=1}^{nd} \phi_d = 1 \tag{1}$$

where, ϕ represents the volume fractions of the phase and the subscript V denotes the continuous (vapor) phase. The index d refers to one or several (nd) dispersed liquid phases (i.e. droplets).

Equations for conservation of mass for continuous (vapor) and dispersed (droplet) phase are given below:

$$\frac{\partial(\phi\rho)_V}{\partial t}+\frac{\partial(\phi\rho u_j)_V}{\partial x_j}=-\sum_{d=1}^{nd}\dot{m}_d-\sum_{d=1}^{nd}m_{crit}\phi_V J_d \tag{2}$$

$$\frac{\partial(\phi\rho)_d}{\partial t}+\frac{\partial(\phi\rho u_j)_d}{\partial x_j}=-\sum_{d=1}^{nd}\dot{m}_d-\sum_{d=1}^{nd}m_{crit}\phi_V J_d \tag{3}$$

whereas $\dot{m}$ is mass condensed on an already existing droplet is a source term, J_d is nucleation rate and mass of the critical droplet is m_{crit}, ρ is the density and u is the flow velocity. The mass conservation for the mixture is expressed by the equation below:

$$\frac{\partial\rho}{\partial t}+\frac{\partial(\rho u_j)}{\partial x_j}=0 \quad where \quad \rho u_j=(\phi\rho u_j)_V+\sum_{d=1}^{nd}(\phi\rho u_j)_d \tag{4}$$

An assumption is made that the droplets are small enough to follow the vapor without slip. Hence, no drag forces between the phases. Then it is sufficient to solve only the momentum equation for the continuous vapor phase which equates to

$$\frac{\partial(\phi\rho u_j)_V}{\partial t}+\frac{\partial(\phi\rho u_j u_i)_V}{\partial x_j}=-\phi_V\frac{\partial p}{\partial x_i}_{i,d}+\frac{\partial(\phi\tau_{ij})_V}{\partial x_j}-\sum_{d=1}^{nd}\dot{m}_{V/d}u \tag{5}$$

whereas τ_{ij} is the viscous stress tensor and the source term $\dot{m}_{V/d}$ is the inter-phase mass transfer. The energy conservation equation for the continuous vapor phase is given by:

$$\frac{\partial(\phi\rho H)_V}{\partial t}+\frac{\partial(\phi\rho u_j H)_V}{\partial x_j}=\phi_V\frac{\partial p}{\partial t}+\frac{\partial}{\partial x_j}\left(\phi\Gamma_t\frac{\partial T}{\partial x_j}\right)_V+\frac{\partial(\phi u_i\tau_{ij})_V}{\partial x_j}-\sum_{d=1}^{nd}S_{H,d} \tag{6}$$

whereas H is the total enthalpy, Γ_t is the thermal diffusion coefficient and S_H is the source term that includes the effects of mass and heat transfer. For the dispersed phase the energy conservation equation is replaced by the simple algebraic formulation,

$$T_d=T_s(p)-\Delta T\left(\frac{r_{crit}}{r}\right) \tag{7}$$

Equation (7) is used to calculate the droplet temperature. This approach is feasible for droplets with a diameter below 1 μm. If the droplet size exceeds 1 μm an additional transport equation for the dispersed phase has to be solved [11, 20].

2.2 Non-equilibrium (NES) Model

Several researchers worked on the mathematical model of droplet formation rates [2, 3, 7, 21, 23]. The process of droplet formation is known as a classical homogenous nucleation theory. The number of droplets formed per unit volume and unit time is given below:

$$J = \frac{q_C}{1+\eta}\sqrt{\frac{2\sigma}{\pi m^3}}\frac{\rho_V^2}{\rho_d}\exp\left(-f\frac{4\pi\sigma r_{crit}^2}{3KT_V}\right) \qquad where \qquad \eta = 2\frac{\gamma-1}{\gamma+1}\frac{L}{RT_V}\left(\frac{L}{RT_V}-\frac{1}{2}\right) \tag{8}$$

where, q_c is condensation coefficient and is normally set to unity, m is the mass of one water molecule and K is Boltzmann's constant. η is defined as non-isothermal correction of Kantrowitz [16] and is defined as the ratio of specific heats and the latent heat. The correction factor 'f' is introduced to give an opportunity for engineers to calibrate the nucleation rate as presented in the validation of the wet steam model section.

In eq. (9), ν is a function of α . α is an empirical constant used to fit numerical calculations to measurements. It's value varies from 0 to 9. Young model [23] to predict the droplet growth is given by:

$$L\rho_d\frac{dr}{dt} = \frac{\lambda_c}{r}\frac{1}{1/(1+2\beta Kn)+3.78(1-\nu)(Kn/\mathrm{Pr})}\times(T_s(p)-T_v)(1-r_{crit}/r) \tag{9}$$

Conservation of the droplet number N_d is considered for the two-phase flow. For each dispersed phase an additional equation is considered:

$$\frac{\partial(\rho N)_d}{\partial t}+\frac{\partial(\rho u_j N)_d}{\partial x_j} = \phi_V\rho_d J_d \tag{10}$$

Here, ρu_j is the weighted velocity.

2.3 Boundary Condition and Settings

For the current study four properties, namely the flow direction (two directions in 2D flow), stagnation temperature and stagnation pressure must be specified at the inlet. The boundary at the outlet is supersonic. The flow field property (density) is extrapolated from the numerical solution. SST turbulence model is used with turbulence intensity of 5-10% [1, 7, 19].

3. Convergence and Mesh Independency Study

Convergence criteria with an RMS value of $1e^{-6}$ obtained for steady and $1e^{-5}$ is for unsteady simulation. For unsteady simulation the time step of $5E^{-7}s^{-1}$ and coefficient loop of 5-20 is used depending on the transient simulation case [1, 8, 15].

Table 1: Convergence study for with steady simulation

	2D Mesh Density					
Temp	5k Mesh	21k Mesh	43k Mesh	77k Mesh	120k Mesh	235k Mesh
100.2°C	√	√	√	x	x	x
102.2°C	√	√	√	√	x	x
103.2°C	√	√	√	√	√	x
105.2°C	√	√	√	√	√	√
112.2°C	√	√	√	√	√	√
NOTE: √ = Solution converged with steady state simulations x = Solution converged only with unsteady simulations						

Mesh convergence using steady simulations was carried out for 2D and 3D meshes. It was found that for the finer mesh with lower superheated inlet temperature the convergence is not achieved using steady state flow simulations. Comparing the pressure distribution and droplet diameter mesh with 77k elements for 2D and 3M elements for 3D is considered to be the best resolved mesh.

4. Nozzle Geometries

4.1 Experimental Nozzle

Fig. 3 is the Barschdorff nozzle. The radius of the wall curvature of 584mm and the critical throat height of 60 mm. An airfoil section runs along the channel width which is used to support pipe with pressure probe that runs along the channel axis.

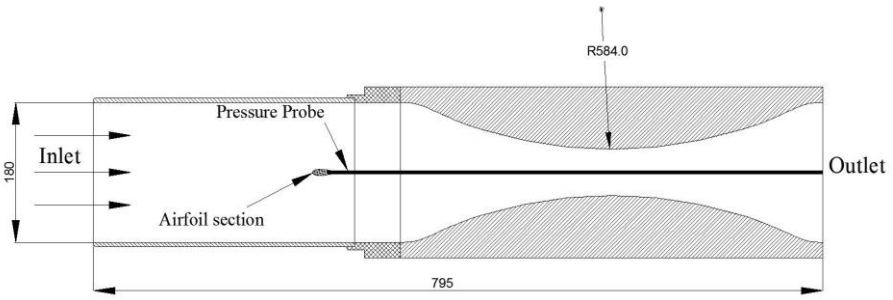

Fig. 3: Barschdorff´s nozzle profile

The wall friction has a direct influence on the spontaneous condensation process and therefore it is important for an accurate friction prediction while designing Laval nozzles [19, 24]. The selection of experimental steam nozzle can be done in two ways as it is very important to note down that the profile of the nozzle is critical. The first approach is designing a new steam nozzle using numerical analysis (e.g. CFD codes) in order to ensure that the nozzle is not too unstable or highly influenced by friction. Or the alternative approach is to study the previously studied nozzles (as it has been done here) and validate with the results available in the literature. The second approach offers more usefulness as one can compare the experimentally computed results with results from others. This can be very useful as it helps to do progressive studies (knowing the drawbacks of past experiments can be improved for new one) on the experimental and numerical sides.

4.2 3D Computational Nozzle

The 3D computational domain contains rectangular inlet geometry with pneumatic mounts (i.e. a pressure probes and airfoil section far upstream the throat that passes across the channel width to support the probe). The location of the leading edge of the airfoil is 389.5mm upstream the throat. A pressure probe has a diameter of 4mm and runs along centerline of the axis of the channel. Fig. 4 shows the 3D computational model in which the width of the channel is 100mm.

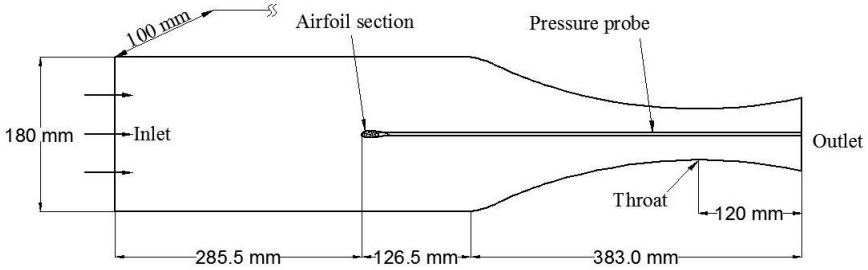

Fig. 4: Dimensions of 3D computational Domain

The outlet of the 3D computational nozzle is truncated 120mm downstream the throat to avoid potential flow instabilities downstream the nozzle.

4.3 2D Computational Nozzle

Fig. 5 shows the section of the 2D nozzle used in the computational domain. The nozzle is truncated 210mm upstream and 120mm downstream of the nozzle throat. The critical height of the throat (y*) is 60mm.

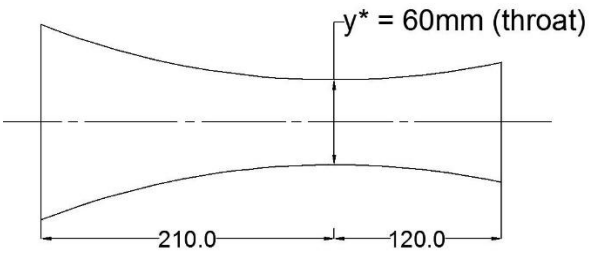

Fig. 5: Dimensions of 2D Computational Domain

The nozzle is shortened for two major purposes, first short nozzle geometry reduces the computational domain and hence ultimately requires less computing power. Secondly, flow becomes more and more unstable as we go downstream the throat and convergence is very difficult to obtain.

5. Results

5.1 Comparison of 2D and 3D results

The influence of boundary layer near the pipe and the wall are significant. Also there is possibility of 3D flow near to the pipe. The results obtained at location L 01 in (Fig. 6) from 3D simulation is used to compare with 2D simulated results. Fluid particles in the core flow are assumed to experience the same pressure variation, but those particles passing close to the blade surface suffer greater entropy production. This results in higher static temperatures than those that pursue nearly isentropic paths through the central portions of the blade passages. Particles which suffer high loss nucleate later in the turbine than those that experience little dissipation [7, 8]. In Fig. 7, the pressure and droplet distribution at different locations on the centerline of the 3D nozzle. There is negligible different in pressure distributions at the three different locations (L 00, L 01, L02) for higher inlet temperature (i.e. 112.2°C).

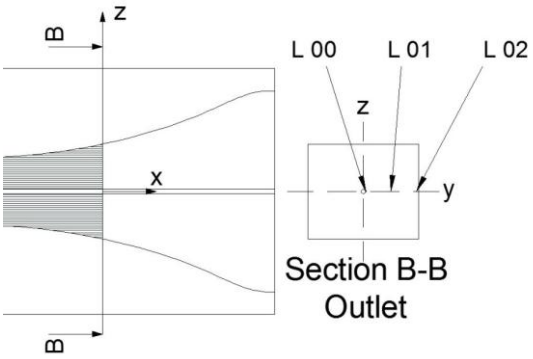

Fig. 6: 3D result analysis

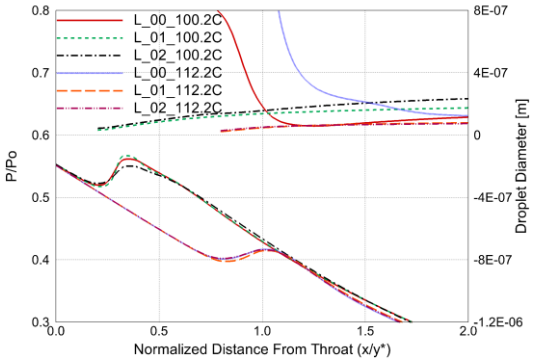

Fig. 7: 3D results

The droplet diameter is widely dispersed at these locations. It can be seen that the droplet formation and growth at the location near to the pipe (L 00) is highly influenced by the wall friction. The frictional losses at walls results in rise of enthalpy and entropy causing the steam to nucleate far downstream at L 00 and L 02 compared to core flow at L 01. Fig. 8 and fig. 9 shows the pressure and droplet diameter distribution along the centerline of 2D and 3D nozzle. The location of the Wilson's point is located at the same location for both 2D and 3D results. Strength of condensation is higher for 2D case compared to 3D. This is consistent with the fact that the loss and dissipation in the 3D nozzle is higher than the 2D nozzle because of the pneumatic mounts. Droplet diameter in 3D nozzle is larger than in the 2D nozzle. In 3D model the nucleation rate is lower, and hence the total droplet number is lower. From Mollier chart the wetness factor is governed by temperature and pressure. The droplet diameter is inversely

proportional to droplet number given that wetness fraction is constant. In 2D model the droplet number is higher than 3D, but the wetness fraction is similar in both models. This explains the reason for having larger droplet sizes in 3D cases compared to 2D.

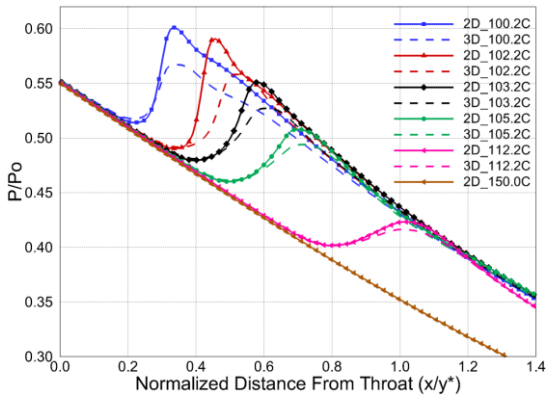

Fig. 8: Pressure distribution

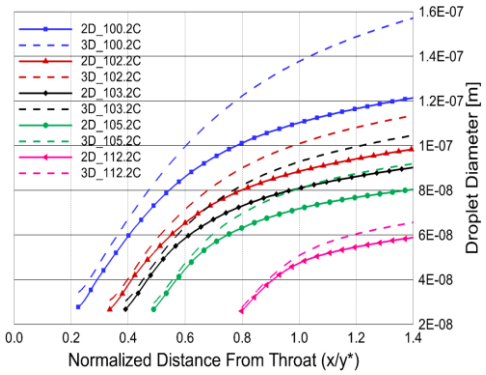

Fig. 9: Droplet size distribution

Onset the nucleation process, the size of the initial droplets is 0.2 – 0.3 µm which then gradually increases downstream the nozzle.

5.2 Validation

The nucleation model in Ansys CFX predicts the Wilson point far ahead of the experimental result. Modified nucleation model with correction factor 'f' is used to fit the CFD with experimental results. In order to fit the Wilson's point different correction factor 'f' in the Young's model is used. With larger correction factor, the strength of nucleation and pressure rise in region of condensation decreases.

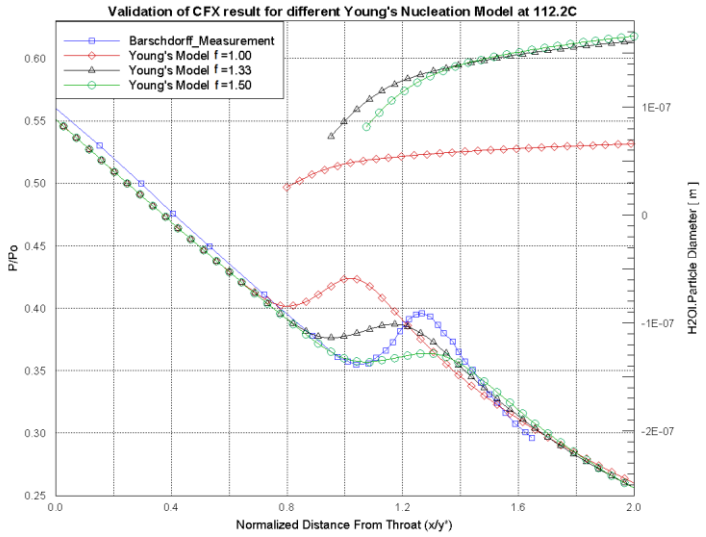

Fig. 10: Validation of CFX result for different Young's Nucleation Model at 112.2°C

The correction factor of 1.33 is used for Moss and Stein Nozzle at inlet conditions of 0.358 bar and 95.15°C [18]; and for Barschdorff nozzle of current work with inlet condition of 0.7839 bar and 112.2°C the correction factor is 1.50. This marks a question in the consistency of correction factor used in the nucleation models used.

5.3 Unsteady Results

At lower super-saturation, the flow filed becomes unstable, resulting in oscillation of the nucleation zone. Fig. 12 shows the oscillation of pressure field, along the centreline of the 2D Laval nozzle. The oscillation of the nucleation zone has been noted by Barschdorff [3, 4]. Also the oscillation of pressure field for total inlet condition of 97.0°C and 0.7893 bar with supersonic nozzle. The computed amplitude of oscillation of the pressure field is 18 mbar which is up to 2.3% of the total inlet pressure and frequency of oscillation is 400 - 500 Hz. Fig. 11 shows the time history of the pressure field oscillation at the centreline and 40mm downstream the throat. The number of iterations required for unsteady simulations in Ansys CFX 16 is very high (i.e. up to 84,000 iterations).

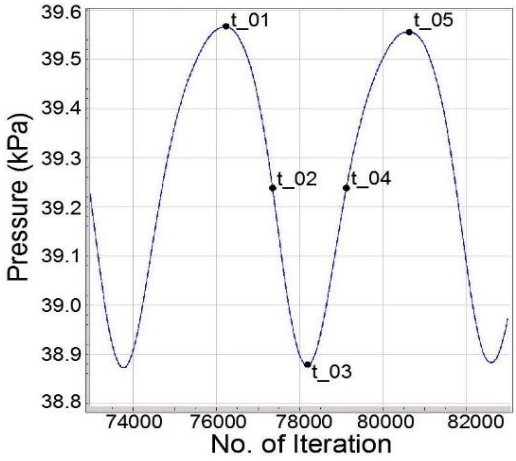

Fig. 11: Pressure field on centerline and 40mm downstream the throat

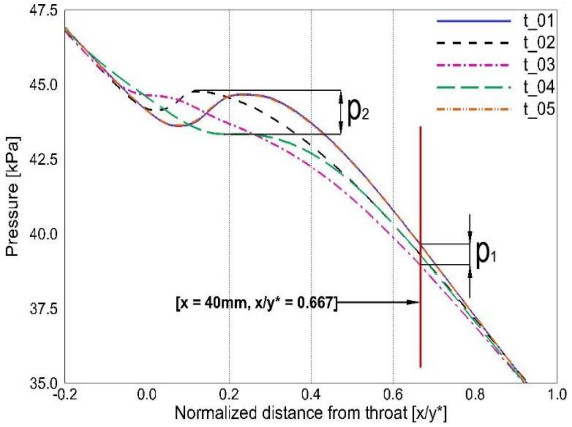

Fig. 12: Unsteady pressure distribution along centerline of 2D nozzle at different time interval

6. Conclusion

Convergence is not obtained for very fine meshes at lower total inlet temperatures (e. g. 120k elements and 100.2°C total inlet temperature) with steady simulation. It is possibly due to the ability of fine mesh to capture very small unsteadiness. Variation of Wilson pressure, Wilson point location and maximum sub-cooling for 2D and 3D model is less than 2%. The deviation in droplet diameter at outlet is up to 18% and in maximum nucleation rate is up to 54% between two case simulations. Difference in 2D and 3D results for maximum nucleation rate is because of the dissipation from airfoil section in 3D simulation. Nucleation zone predicted by Ansys CFX is far upstream and stronger compared to the experimental one. Ansys CFX16 is not able to capture the experimental location of nucleation zone. Maximum amplitude of unsteady pressure value at

97.0°C and 0.7839 bar is about 1.8kPa (=18mbar i.e. about 2.3% of inlet pressure). This force of unsteady condensation is harmful for blade's structural health. The correction factor 'f' in nucleation model depends on boundary condition and nozzle geometry and hence is not a unique value.

References

[1] ANSYS CFX solver manual (2015), Southpointe, Canonsburg, USA.

[2] Bakhtar F et al. (1993), An investigation of nucleating flows of steam in a cascade of turbine blading, *Transaction of the ASME,* **115:** 128 – 134.

[3] Barschdorff D (1971), Verlauf der Zustandsgrössen und gas-dynamische Zusammenhänge bei der spontanen Kondensation reinen Wasserdampfes in Lavaldüsen. *Forsch. Ing.-Wes*. **37:** 146 – 157.

[4] Barschdorff D, Hausmann G and Ludwig A (1976), Flow and drop size investigations of wet steam at sub- and supersonic velocities with the theory of homogenous condition. PRACE INSTYTUTU MASZYN PRZEPŁYWOWYCH: 240 - 257

[5] Chandler K, White A and John Y (2014), Non-equilibrium wet-steam calculation of unsteady low-pressure turbine flows *Proc IMechE Part A: J Power and Energy*, **228(2):** 143–152.

[6] Dykas S (2011), Single- and two-fluid models for steam condensing flow modeling, *International Journal of Multiphase Flow* **37:** 1245 – 1253.

[7] Gerber AG and Kermani MJ (2004), A pressure based eulerian–eulerian multi-phase model for non-equilibrium condensation in transonic steam flow, *Int. J. of Heat and Mass Transfer* **47:** 2217 – 2231.

[8] Gerber AG (2008), Inhomogenous multi-fluid model for prediction of non-equilibrium phase transition and droplet dynamics *Trans, ASME, J. Fluids Eng*. **130(3):** 1-11

[9] Grübel M et al. (2015), Two-phase flow modeling and measurements in low-pressure turbines—part I: numerical validation of wet steam models and turbine modeling, *Journal of Engineering for Gas Turbines and Power,* **137(4):** 042602-042602-11.

[10] Guha A (1997), Analysis and computation of non-equilibrium two-phase flows, *Sadhana*, **22(3**): 295 – 321.

[11] Guha A and Young J (1994), The effect of flow unsteadiness on the homogenous nucleation of water droplets in steam turbines *Philosophical Transactions: Physical Sci. and Engineering*, **349:** 445 – 472.

[12] Gyamathy (1962), Grundlangen einer theorie der nabdampfturbine Doctoral Thesis, Eidgenossischen Technischen Hochschule in Zurich.

[13] Hill PG (1966), Condensation of water vapor during supersonic expansion in nozzles, *J. Fluid Mech*, **25(3):** 593 – 620.

[14] Jonas O (1998), Condensation in steam turbines – new theory and data.

[15] JU Feng-ming, YAN Pei-gang and HAN Wan-jin (2012), Numerical investigation on wet steam non-equilibrium condensation flow in turbine cascade, *Journal of Thermal Science,* **21(6)**: 525-532.

[16] Kantrowitz A (1951), Nucleation in very rapid vapor expansions, *J. Chem Phys.* **19:** 1097 – 1100.

[17] Lee Byeong-Eun, Riu Kap-Jong, Se-Hyun Shin and Soon-Bum Kwon (2003), Development of a Water Droplet Erosion Model for Large Steam Turbine Blades, *ASME International Journal*, **17(1)**: 114-121.

[18] Moses CA and Stein GD (1978), On the growth of steam droplets formed in a Laval nozzle using both static pressure and light scattering measurements, *Journal of Fluid Engineering,* **100:** 311 – 322.

[19] Starzmann J et al. (2014), On kinematic relaxation and deposition of water droplets in the last stages of low pressure steam turbines, *Journal of Turbomachinery*, **136**: 071001-071001-10

[20] Wagner W, Cooper JR, Dittmann A, Kijima J et al. (2000), The IAPWS industrial formulation 1997 for the thermodynamic properties of water and steam *Transactions of the ASME,* **150:** 122 – 182.

[21] White AJ (1992), Condensation in steam turbine cascades, University of Cambridge, UK

[22] White AJ and Young JB (2008), Transient calculations of nucleation and droplet growth for wet-steam expansions *ICPWS XV Berlin*.

[23] Young JB (1992), Two-dimensional, non-equilibrium, wet-steam calculations for nozzles and turbine cascades, *Journal of Turbomachinery,* **114:** 569-579.

[24] Young JB (1995), Wet-steam research at Cambridge 1980-1995 *EPRI Workshop on 'Moisture Nucleation in Steam Turbines' Rochester, New York, USA*.